



*INTERNATIONAL JOURNAL of ELECTRONICS,
MECHANICAL and MECHATRONICS ENGINEERING*

Year: **2019** Volume **9** Number **3**

**International Journal of Electronics, Mechanical and Mechatronics
Engineering (IJEMME)**

PRESIDENT

Doç. Dr. Mustafa AYDIN Istanbul Aydın University, TR

HONORARY EDITOR

Prof. Dr. Hasan SAYGIN Istanbul Aydın University, TR

EDITOR

Prof. Dr. Hasan Alpay HEPERKAN
Istanbul Aydın University, Faculty of Engineering
Mechanical Engineering Department
Florya Yerleskesi, Inonu Caddesi, No.38, Kucukcekmece, Istanbul, Turkey
Fax: +90 212 425 57 59 - Tel: +90 212 425 61 51 / 22001
E-mail: hasanheperkan@aydin.edu.tr

ASSISTANT EDITOR

Prof. Dr. Oktay ÖZCAN
Istanbul Aydın University, Faculty of Engineering
E-mail: oktayozcan@aydin.edu.tr
Ass. Prof. Eylem Gülce ÇOKER
Istanbul Aydın University, Faculty of Engineering
E-mail: eylemcoker@aydin.edu.tr

EDITORIAL BOARD

AYDIN Nizamettin	Yildiz Technical University, TR
CATTANI Carlo	University of Salerno, ITALY
CARLINI Maurizio	University "La Tuscia", ITALY
CHAPARRO Luis F.	University of Pittsburg, USA
DIMIROVSKI Gregory M.	SS C. and Methodius University, MAC
HARBA Rachid	Orleans University, FR
HEPBAŞLI Arif	Yaşar University, TR
JENANNE Rachid	Orleans University, FR
KOCAKOYUN Şenay	Istanbul Aydın University, TR
KONDOZ Ahmet	University of Surrey, UK
RUIZ Luis Manuel Sanches	Universitat Politècnica de València, Spain
SIDDIQI Abul Hasan	Sharda University, Indian
STAVROULAKIS Peter	Telecommunication System Ins., GR

ADVISORY BOARD

AKAN Aydın	Istanbul University, TR
AKATA Erol	Istanbul Aydın University, TR
ALTAY Gökmen	Bahcesehir University, TR
ANARIM, Emin	Bosphorus University, TR
ASLAN Zafer	Istanbul Aydın University, TR
ATA Oğuz	Istanbul Aydın University, TR
AYDIN Devrim	Dogu Akdeniz University, TR
BAL Abdullah	Yildiz Technical University, TR
BİLGİLİ Erdem	Piri Reis University, TR
CEKIÇ Yalcin	Bahcesehir University, TR
CEYLAN Murat	Konya Selcuk University, TR
DOĞRUEL Murat	Marmara University, TR

EI KAHLOUT Yasser	TUBITAK-MAM, TR
ERSOY Aysel	Istanbul University, TR
GÜNERHAN Huseyin	Ege University, TR
GÜNAY Banihan	University of Ulster, UK
GÜNGÖR Ali	Bahcesehir University, TR
HEPERKAN Hasan	Istanbul Aydın University, TR
KALA Ahmet	Istanbul University, TR
KAR A. Kerim	Marmara University, TR
KARAMZADEH Saeid	Istanbul Aydın University, TR
KARAÇUHA Ertuğrul	Istanbul Technical University, TR
KARAOCA Adem	Bahcesehir University, TR
KARAKOÇ Hikmet	Anadolu University,TR
KARTAL Mesut	Istanbul Technical University, TR
KENT Fuad	Istanbul Technical University, TR
KILIÇ Niyazi	Istanbul University,TR
KINCAY Olcay	Yildiz Technical University, TR
KUNTMAN Ayten	Istanbul University, TR
KOCAASLAN İlhan	Istanbul University, TR
ÖNER Demir	Maltepe University, TR
ÖZ Hami	Kafkas University, TR
ÖZBAY Yüksel	Konya Selçuk University, TR
PAKER Selçuk	Istanbul Technical University, TR
PASTACI Halit	Halic University, TR
SAYAN Ömer F.	Telecommunications Authority, TR
ŞENER Uğur	Istanbul Aydın University, TR
SİVRİ Nuket	Istanbul University, TR
SÖNMEZ Ferdi	Istanbul Arel University, TR
SOYLU Şeref	Sakarya University, TR
UÇAN Osman Nuri	Istanbul Kemerburgaz University, TR
UĞUR Mukden	Istanbul University, TR
YILMAZ Aziz	Air Force Academy, TR
YILMAZ Reyat	Dokuz Eylül University, TR

VISUAL DESIGN & ACADEMIC STUDIES COORDINATION OFFICE

Nabi SARIBAŞ - Selin YILMAZ - Elif ERMAN

PRINTED BY

Renk Matbaası Basım ve Ambalaj San. Tic. A.Ş.

Ziya Gökalp Mah. Süleyman Demirel Bulvarı İş Modern D Blok No:27D D:D8 34104 Başakşehir / İstanbul

ISSN: 2146-0604

International Journal of Electronics, Mechanical and Mechatronics Engineering (IJEMME) is peer-reviewed journal which provides a platform for publication of original scientific research and applied practice studies. Positioned as a vehicle for academics and practitioners to share field research, the journal aims to appeal to both researchers and academicians.

Internationally indexed by EBSCO and DOAJ

CONTENTS

From the Editor

Prof. Dr. Hasan Alpay HEPERKAN

Cyber Security Algorithm Development For Microgrid And Smart Grid Systems

Ahmet DURMUŞ, Mehmet Emin TACER1687

Autonomous Photovoltaic Solar Cell Using Tracking System Design and Implementation

Metin BİLGİN, Kübra ÇELEBİ1697

New Control Method For Dual Voltage Rectifier

Rai Muhammad OMAR, Murtaza FARSADI1705

From the Editor

International Journal of Electronics, Mechanical and Mechatronics Engineering (IJEMME), is an international multi-disciplinary journal dedicated to disseminate original, high-quality analytical and experimental research articles on Robotics, Mechanics, Electronics, Telecommunications, Control Systems, System Engineering, Biomedical and Renewable Energy Technologies. Contributions are expected to have relevance to an industry, an industrial process, or a device. Subject areas could be as narrow as a specific phenomenon or a device or as broad as a system.

The manuscripts to be published are selected after a peer review process carried out by our board of experts and scientists. Our aim is to establish a publication which will be abstracted and indexed in the Engineering Index (EI) and Science Citation Index (SCI) in the near future. The journal has a short processing period to encourage young scientists.

Prof. Dr. Hasan HEPERKAN
Editor





A New Patch Antenna Design for X Band Applications

Cemal İBRAHİMPAŞA¹, Saeid KARAMZADEH²

Abstract—in the last years the rapid development in the satellite communication and broadcasting systems require to develop a low cost, light weight, easiness in movement and in usage antennas. That's capable of high performance at the same time. In this paper X-band micro-strip antenna has been discussed and designed which could be used for many applications and it is consist of radiating patch on a Roger RO4003C substrate with a ground patch, and the micro-strip feeding line to the patch is set on 50 Ohm. And it will give us 8.45 dB peak gain in X-band Frequency range and wide Impedance Bandwidth (IBW) range from 5.8 GHz till 12 GHz.

Keywords: patch antenna, X-band.

I. INTRODUCTION:

These days the rapid development in the wireless communication

systems and the importance of providing high quality multimedia services for our daily life activities requires to keep developing antennas that's easy to use and easy to fabricate at the same time. The huge demands on the satellites communication services require us to develop our systems and antennas as it will receive and send the electromagnetic waves to be able to use every possible range of frequency [1]. The range of X-Band is (8-12) GHz this band is mainly used by the military especially in radar applications but also the X-band is used in civil, and government applications such as television broadcasting, weather forecast, and for air traffic control and vehicle speed detection. And it has many advantages like not been affected by weather conditions and its high throughput which make it very suitable to be used to send High Definition HD videos, voice and data [2]. The micro-strip antenna is made of a radiated metallic piece (patch) which is printed or

¹ *Electrical and Electronics Engineering, Engineering Faculty, Istanbul Aydin University, Istanbul, Turkey, jamalbasha@stu.aydin.edu.tr*

² *Electrical and Electronics Engineering Department, Faculty of Engineering and Natural Sciences, Bahçeşehir University, Istanbul, Turkey, <https://orcid.org/0000-0003-0669-0746>, karamzadeh@itu.edu.tr*

attached on a dielectric material [3]. Also it's called as dielectric substrate and on the bottom side of the dielectric substrate attached a ground patch that will be separated from the upper patch with the dielectric substrate, this radiated patch could be designed into many configurations and shapes, the most used shapes are the circular and the rectangular patch [4].

The aim of this letter is to present a single element patch antenna that will be operate on x-band frequency and that have a rectangle holes in the ground slot to increase the return lose value and a pair of notches had been made on the lower corner of the patch to achieve maximum impedance matching [5]. The antenna design and simulation done by using Computer Simulation Technology (CST) studio software.

II. ANTENNA DESIGN:

The micro-strip antenna substrate is build using Rogers RO4003C material which is a glass reinforced hydrocarbon/ ceramic laminates designed for high volume commercial application and this material is designed to offer a superior high frequency range performance. Also, comparing to the FR4 material the RO4003C has a low dielectric tolerance and loss which gave it the excellent performance in the high frequencies. Its relative permittivity $\epsilon_r = 3.55$, and the dielectric loss tangent is $\delta = 0.0027$ [6]. The size of our designed antenna is $40 \times 38 \times 1.524 \text{ mm}^3$ which means that the width of the antenna is 40 mm and the length is 38 mm and the antenna thickness of the substrate is 1.524 mm. The patch will consist of main rectangular part adjoined by smaller rectangular parts to form two notches from both sides on upper face of the substrate to operate effectively on the higher estimated frequency and to give us mush enhanced impedance bandwidth [7]. While on the ground face of the substrate we have a rectangle patch and a rectangular slot had been cut from in addition that the width of the ground slot is not equal to the upper patch to give more stability and wider bandwidth response in X-band frequency range. The radiating patch will be feed with 50Ω . The antenna feeding done by a using the feed line method where the feed line will be attached to the patch on the upper face of the antenna [8] and that will provide a planer structure. So, the fabrication will be easier. The antenna design with its first step and the last refined design is shown in figure 1 and figure 2 respectively.

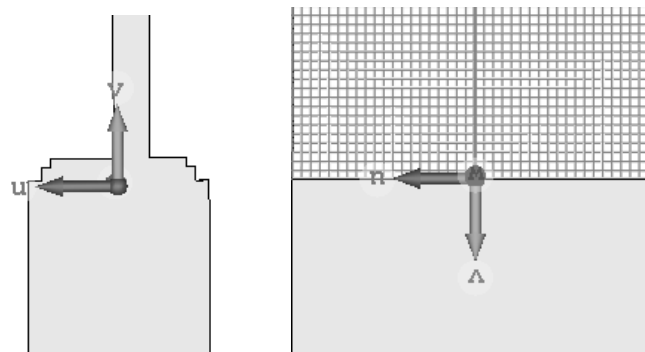


Figure 1. The first step of the designed antenna

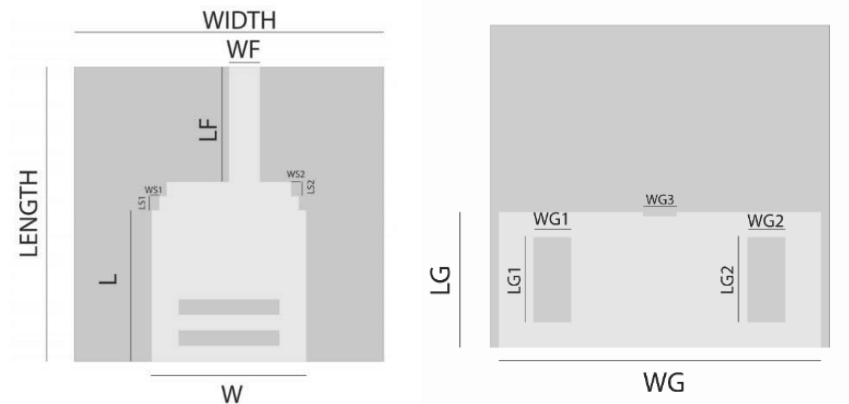


Figure 2. The final design of the antenna

Table 1. The Designed Antenna Dimension

Parameters	Values (mm)	Parameters	Value (mm)
Sub Width	40	WF	4
Sub Length	38	LF	16
Sub high	1.524	WS1	1.5
W	20	LS1	1.5
L	19.5	WS2	1
WC	3.8	LS2	1
LC	2.7	Mt	0.1
LS3	2	WS3	13
LS4	2	WS4	13
WG	38	LG	16
WG1	4.5	LG1	10
WG2	4.5	LG2	10
WG3	4	LG3	0.5

III. ANTENNA SIMULATICON AND RESULTS:

This paper aims to present a single element patch antenna to be used in the X-band frequency applications and to check our antenna efficiency within this frequency range. The results will be studied and observed of the following antenna parameters.

A. Return Lose and VSWR:

The return loss (S11) shows how good is the matching between the transmission line and the antenna [9]. At first, we had the good value only on a very narrow bandwidth; by cutting the side edge from the ground slot we got enhanced S11 on much wider bandwidth. Because these cuts helped to improve the electromagnetic coupling between the upper patch and the ground slot [10], as it shows in the figure 3 that in the first stage the good value of S11 was just close to 9.8 GHz with very narrow band while the value was very low for the other frequency range. On the other hand, when the ground slot had been refined the S11 value improved to had good value from 5.8 GHz till 11.8 GHz. Moreover, the return loss result should be less than -10 DB for an effective antenna [11]. Figure 4 illustrate the value of S11 in our design. The antenna reference impedance is constant on 50 Ohm.

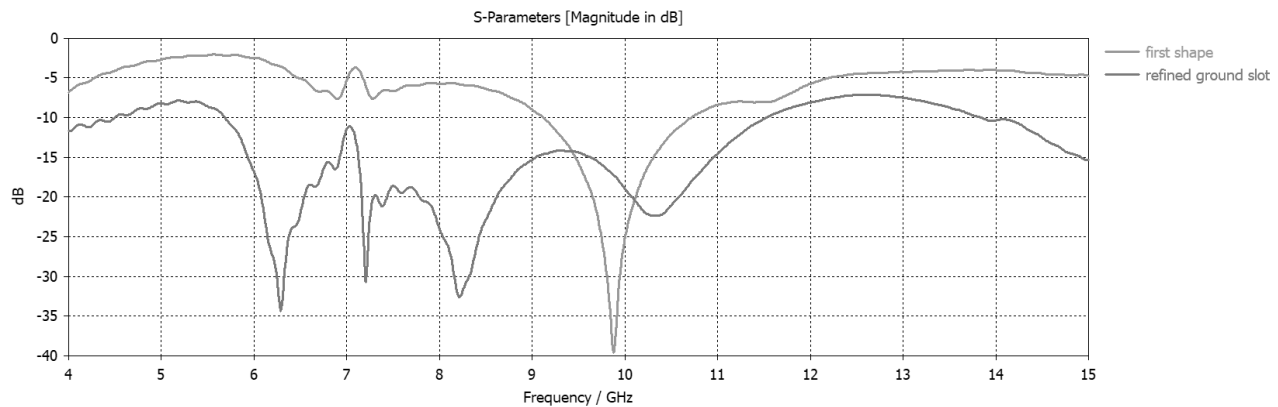


Figure 3 The designed antenna S11 comparison with the result of the same design before the ground slots refining.

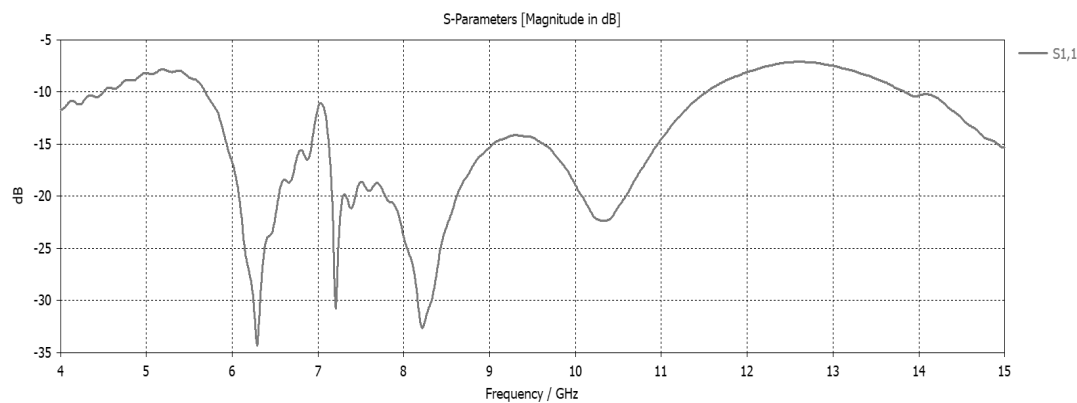


Figure 4 The designed antenna S11 Diagram

As S11 of the designed antenna had been analyzed let's compare VSWR results in the main step of our antenna design with the final shape as we can see in the figure 4 that in the beginning before refining the design of the ground slot we had a narrow bandwidth impedance which was between 9-11 GHz and this small range will not allow us to use our antenna in many X Band application but

after the cut of the Ground slot the bandwidth impedance has been improved and we gained a wider bandwidth. Ground slot the bandwidth impedance has been improved and we gained a wider bandwidth from 5.7 till almost 11.8 GHz.

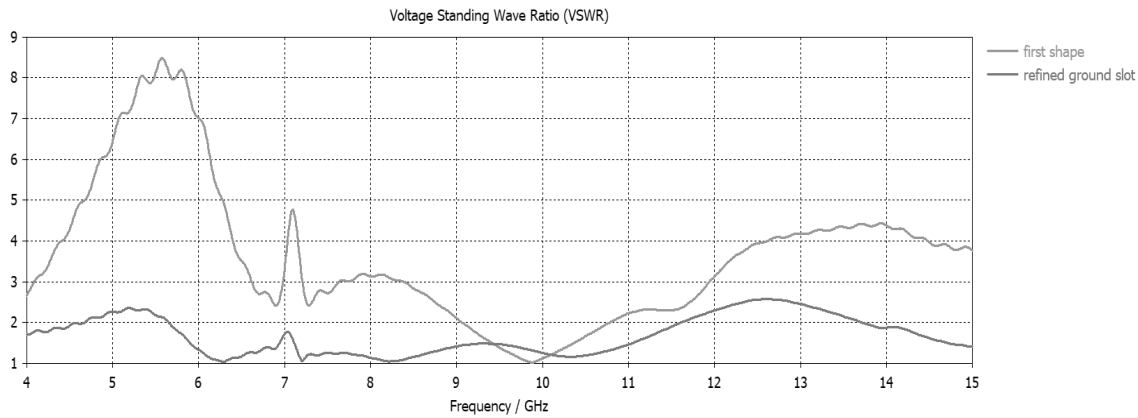


Figure 5 The designed antenna VSWR comparison with the result of the same design before the ground slots refining.

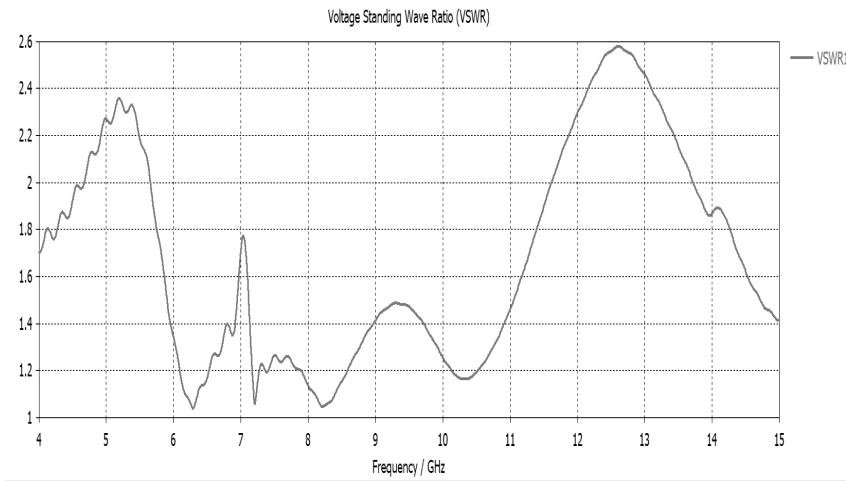


Figure 6 The Designed antenna VSWR

B. Radiation Pattern and Antenna Efficiency :

In the figure 7 the 1-D radiation pattern for our final design of the antenna has been shown as it illustrate the statistics of the ideal main lobe value to the side lobe value.

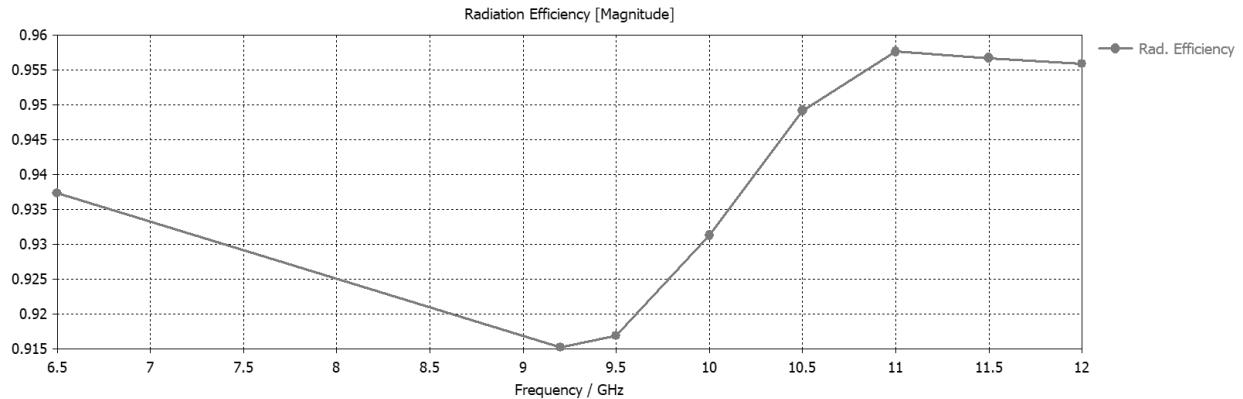


Figure 9 The antenna Radiation efficiency

C. Surface Current Distribution:

The last study that had been done on the antenna is the Surface current distribution, to see the antenna behavior in the final design. Figure 10 illustrate the importance of the distance that had been done between the upper patch and the ground patch which created a current intensity in addition to that in the feedline the current is intensely located and finally the rectangle cuts in the upper face and in the lower face helped with improving the current flow on the patch surface.

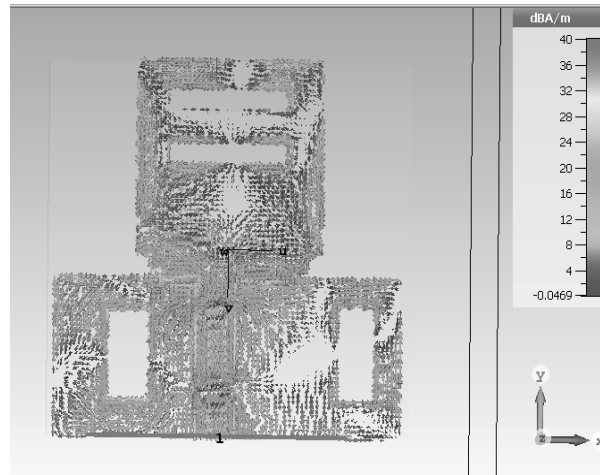


Figure 10 The Designed antenna Surface current distribution

At last the proposed antenna had been compared in terms of dimensions gain frequency range and S11 values with some of other antenna designs, and this references numbers and values are mentioned in the table

Table 2 Comparison between the designed antenna and the references antennas

REF NO	Dimensions (mm)	Center Frequency (GHZ)	Substrate material	Peak GAIN (DB)	S11 (DB)	Disadvantage
[12]	12*18*1.6	10.5	FR4	6.25	-18	
[13]	33.10*16.84*1.57	8.2	FR4	8.6	-58.2	VSWR BW is very narrow
[14]	9.12*7.44*1.6	9.49	FR4	4.31	-23.87	Low gain value
[15]	21.17*21.17*1.535	9.36	RT5880	7.622	-18.81	-
[16]	17.79*21.96*1.588	8.9	RT Duriod	8.15	-16.10	-
[17]	14*16*1.544	9.1	FR4	4.6	-28	Low gain value
[18]	30*30*3	9.5	FR4	4.6	-18	Low gain value
The proposed antenna	40*38*1.524	10.5	RO4003C	8.49	-23	

IV. CONCLUSIONS AND FUTHUER WORK:

In this paper, antenna designing to be used for X-band frequency application had been done by using RT 4003C as a substrate material because of its efficiency results on our desired range of frequencies, then compared that result that we had with the result that we will got if we used the FR4 common material, and found out that the RT 4003C will give better results and stability of this design. A refining of the design in the ground slot had been done to achieve better results. Finally, our antenna is able to achieve around 8.49 dB peak gain on 10.5 GHz which is a X-band Frequency also our antenna has a wide IBW range from 5.8 GHZ till 12 GHZ as the value of VSWR is less than 2 within this range so this antenna could be used effectively with the whole frequency band of the X-band, later on the current surface distribution of the antenna has been analyzed and found out the importance of the rectangular slots that had been done on the radiated patch and on the ground slot of the antenna.

After that a comparing of the results had been done to similar designed antennas that have been used for X-band frequencies. In a conclusion our antenna has a very good results in X-band frequency range and it could be used in many applications that operate at the band range, TV

broadcasting is one of these applications and it could be used in radar applications and many more applications. The antenna design and analysis had been done using CST studio simulation software. For future work we recommend to use our designed antenna as a single element within an array antenna to give a higher gain and to be able to replace other antenna types that give a high gain but have a much bigger physical size compared to an array micro-strip antenna such as the reflector antenna.

V References

- [1] R. K. Crane, Propagation handbook for wireless communication system design, CRC Press, 2003.
- [2] “ESA European space Agency,” 3 october 2018. [Online]. Available: https://www.esa.int/Our_Activities/Telecommunications_Integrated_Applications/Satellite_frequency_bands.
- [3] C. A. Balanis, Antenna theory: analysis and design, John Wiley & Sons, 2016.
- [4] M. S. e. a. Kumar, “Design of microstrip square-patch antenna for improved bandwidth and directive gain,” *International Journal of Engineering Research and Applications (IJERA)*. , 2012.
- [5] K. L. W. a. C. L. T. S. W. Su, “Ultra-wideband square planar monopole antenna for IEEE 802.16a operation in the 2–11 GHz,” *Microw. Opt. Technol. Lett*, vol. 24, pp. 463-466, 2004.
- [6] O. T. N. & A. A. Randy, “Circularly polarized slotted-ground microstrip antennas for radiofrequency identification readers,” *Microwave and Optical Technology Letters*, vol. 54(10), p. 2304–2309, 2012.
- [7] W. C. a. J. C. Jihak Jung, “A Small Wideband Microstrip-fed Monopole Antenna,” *IEEE MICROWAVE AND WIRELESS COMPONENTS LETTERS*, vol. 15, 2005.
- [8] M. K. e. a. Kim, “A T-shaped microstrip-line-fed wide slot antenna,” *IEEE. Antennas and Propagation Society International Symposium*, vol. 3, 2000.
- [9] D. M. Pozar, Microwave engineering, John Wiley & Sons, 2009.
- [10] T. Bird, “Definition and Misuse of Return Loss,” *IEEE Transactions on Antennas and Propagation*, vol. 51(2), pp. 166-167, 2009.
- [11] R. M. Milind Saurabh Singh, “Rectangular Monopole Patch Antenna for for C band and X band Applications,” in *5th IEEE Uttar Pradesh Section International Conference on Electrical, Electronics and Computer Engineering (UPCON)*, 2018.

- [12] A. K. M. S. Divesh Mitta, "High Gain Substrate Slitted Microstrip Patch Antenna Design for X-band Satellite Uplink Applications," in *Progress In Electromagnetic Research Symposium (PIERS)*, Shanghai, China,, 2016.
- [13] R. & S. Kiruthika, "Comparison of different shapes in microstrip patch antenna for X-band applications," in *International Conference on Emerging Technological Trends (ICETT)*., 2016.
- [14] A. S. F. R. U. Z. K. M. I. K. M. A. S. N. & M. H. Iqbal, "Comparative study of micro strip patch antenna for X band using micro strip line feed and coaxial feed.," in *International Conference on Engineering and Emerging Technologies (ICEET)*., 2018.
- [15] A. K. & S. J. S. Sidhu, "Microstrip Rectangular Patch Antenna for S and X band applications," in *International Conference on Wireless Communications, Signal Processing and Networking (WiSPNET)*, 2016.
- [16] P. V. Ankita Sood, "Design of Dual Band Microstrip Patch Antenna for Satellite Communication and Radar Applications," *IJISSET - International Journal of Innovative Science, Engineering & Technology*, vol. 3, no. 4, 2016.
- [17] B. M. R. S. Vivek Singh, "A Compact and Wide Band Microstrip Patch for X-band applications," in *Second International Conference on Advances in Computing and Communication Engineering*, 2015.
- [18] M. J. A. a. Z. N. Chen, "Wideband monopole antennas formulti-band wireless systems," *IEEE Antennas Propagation*, vol. 45, 2003.



IJEMME

Received: 02.06.2019

Accepted: 27.06.2019

Circularly Polarized Patch Antenna Design For C – Band Applications

Setareh SAMADI¹, Saeid KARAMZADEH²

Abstract – This work presents a novel design of a compact ultra-wideband (UWB) coplanar waveguide (CPW)-fed patch antenna that could that cover C-band frequency band. The antenna has a close-packed size of 50 x 50 x 0.8 mm and gives an appropriate impedance bandwidth all over the frequency range of 1.6GHz to 7GHz. The antenna gain has been reached to 5dB. The steps taken in order to achieve the proposed antenna will be discussed in this paper.

Keywords: Patch antenna, CPW, C - band, UWB

1. INTRODUCTION

In a wireless communication system, the increment of the gain of antennas used for communication yields in the increment of the wireless coverage range, minimizes the fallacies, rises possible bit rates and reduces the battery utilization of wireless transmission devices. Matching the polarization between the emitter and the receiver antenna is one of the main items in increasing this gain [1-5]. There are some characteristics that should be the same in both transmitter and receiver antennas to reach this polarization matching such as; spatial orientation, axial ratio (AR), and the same perception of polarization [3-5]. It is almost impractical to continuously match the dimensional orientation of the gadget in transportable wireless application where wireless gadget constantly changes their position and direction. Since the radiated waves keep on oscillating in a ring that is up-right to the direction of generated waves, circular polarization (CP) antennas can be easily matched in a broad scope of orientations [1-6].

Comparing to other kinds of antennas, micro-strip antennas are most repeatedly utilized in applications that require different kinds of polarization. Generally, micro-strip antennas are

¹ *Electrical and Electronics Engineering, Engineering Faculty, Istanbul Aydin University, Istanbul, Turkey.*

² *Electrical and Electronics Engineering Department, Faculty of Engineering and Natural Sciences, Bahçesehir University, Istanbul, Turkey, <https://orcid.org/0000-0003-0669-0746>*

Corresponding Author: Saeid Karamzadeh, E-mail: karamzadeh@itu.edu.tr

advantageous because they can operate in at microwave frequencies where other antennas cannot, they are cheap, light and easy to analysis [1][4][5].

A micro-strip patch antenna with the frequency range of 1.6GHz to 7GHz will be discussed in this paper. This frequency range covers the C-band range which is from 4GHz to 8GHz and also covers the UWB frequency range which is from 3.1GHz to 10.6 GHz. However, the main goal of this paper is to present a novel design of CP patch antenna for C-band(4-8GHz) applications [1-6].

In order to reach this novel antenna design, a survey has taken place comparing the effect of different patch, ground plane and substrate designs on the radiation features of circularly polarized micro-strip antenna. The analyzation of the characteristics parameters such as, VSWR, radiation pattern and return loss are done by HFSS 15.0 software.

2. ANTENNA DESIGN

In this part, the geometrical design of the proposed antenna will be discussed in detail with all the changes and improvements made in order to achieve the proposed antenna. The proposed antenna consists of radiating patch, ground plane, micro-strip feeding line, and a rectangular slot.

Figure1, is an illustration of the proposed antenna, the substrate of this antenna is square-shaped and is made of FR4 material. The square shaped substrate has the length of 50 mm and it's thickness is equal to 0.8mm. The dielectric constant of the substrate is equal to $\epsilon_r=4.4$. The feeding technique that is utilized in this antenna is 50Ω CPW feeding line. The signal strip-line has the width of 3.7mm and also the width of the gaps that are located between the signal strip and the ground plane have the width of 0.55 mm. In order to achieve a wider bandwidth and better axial ratio, an asymmetrical ground plane is designed for this antenna.

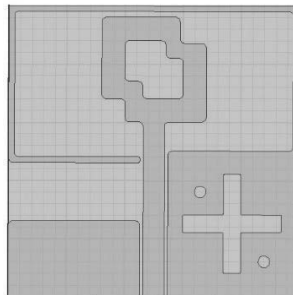


Figure1: The proposed antenna

3. SIMULATION AND RESULTS

Figure 2(a) shows the uncomplicated and simple design of micro-strip antenna which's frequency band is from 1.698 GHz to 4.199GHz and from 4.98GHz to 6.80GHz.

In this part since geometrical configuration of the antenna are calculated. Some of the important characteristic of the antenna such as Return loss (S_{11}), VSWR, Gain, Radiation pattern and Axial

ratio (AR) will be discussed.

In order to achieve the final design, three steps have been taken. The first design is shown in Figure 2(a), In the second step as it is shown in Figure 2(b), to achieve better results than the initial design, defected ground structure (DGS) methods have been used by adding a plus shaped and two circular shaped cuts in the ground plane of the micro-strip antenna. These cuts in the ground plane improve the circular polarization (CP) and also minimizes the inductive characteristics of the patch by producing capacitive loads, also produces resistive input impedance which makes the bandwidth range increase.

In the third step all the corners and edges of the antenna including patch and the ground plane, were rounded. Rounded corners in micro-strip patch antennas yields in a better return loss, flatter input impedance, more stable radiation pattern and uniform distribution of the surface wave at the same time. Figure 2(c) shows the third step of our proposed micro-strip antenna's design.

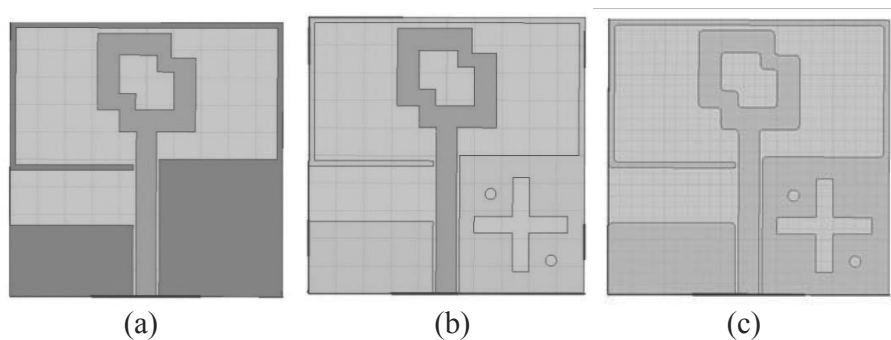
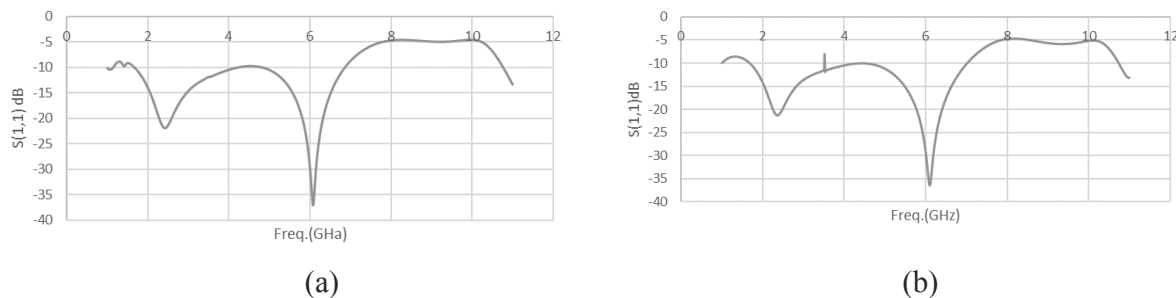
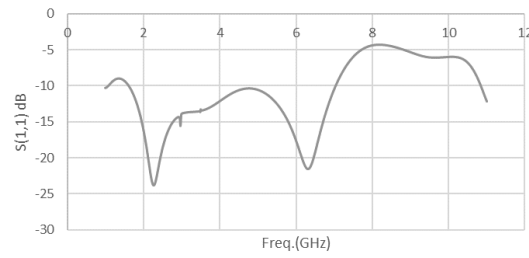


Figure 2: a) The initial design of the proposed antenna b) Micro-strip antenna with plus and circular shaped cuts c)The proposed antenna

This section is comparing some of the general results of all three steps that have been taken to achieve the final design.

The Return Loss (S_{11}) of the three designs has been shown in figure 3. This figure 3(c) indicates that the proposed antenna is operating in 1.612 GHz to 7.173GHz.





(c)

Figure 3: The Return Loss of the a) uncomplicated initial design, b) second design with slots in ground plane and c) proposed antenna with rounded edges

Figure 4 is a comparison between VSWRs of all three antennas that have been designed to achieve the final antenna. As the figure shows, the VSWR bandwidths of these three steps are 5.1GHz, 5.4GHz and 5.6GHz respectively. And the VSWR of the proposed antenna is smaller than 2 (VSWR < 2) at the frequency range of 1.55 GHz to 7GHz.

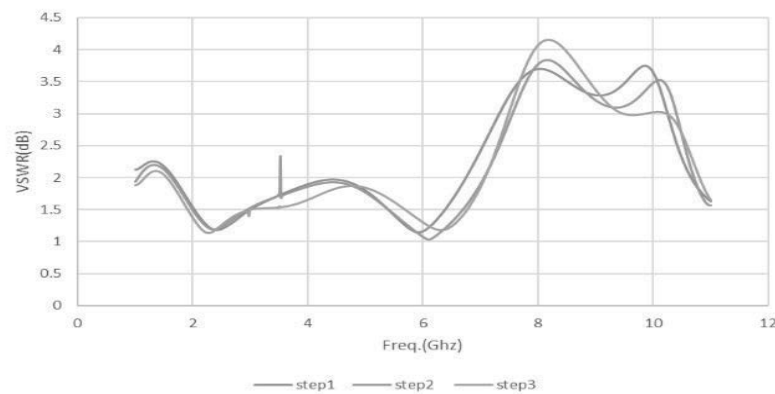


Figure 4: The comparison between VSWRs of all three antennas

Step1: Basic antenna design, Step2: Second design with cuts in the ground plane, Step3: Proposed antenna

For the to Radiation pattern of the proposed antenna, the related measurements have been done at the frequency of 4GHz, also phi is equal to 0 degree and theta is 90 degrees.

As it is shown in figure 5, the last design has the best radiation results comparing to earlier designs. Although their radiation pattern shapes may look like each other, the maximum power radiated by the proposed antenna is higher than the others.

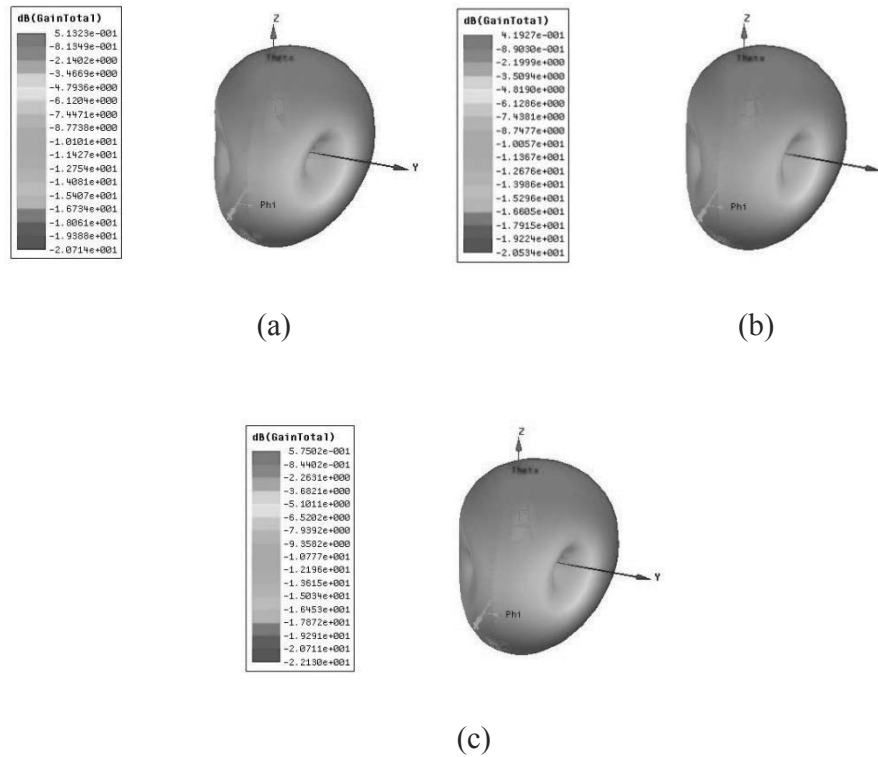
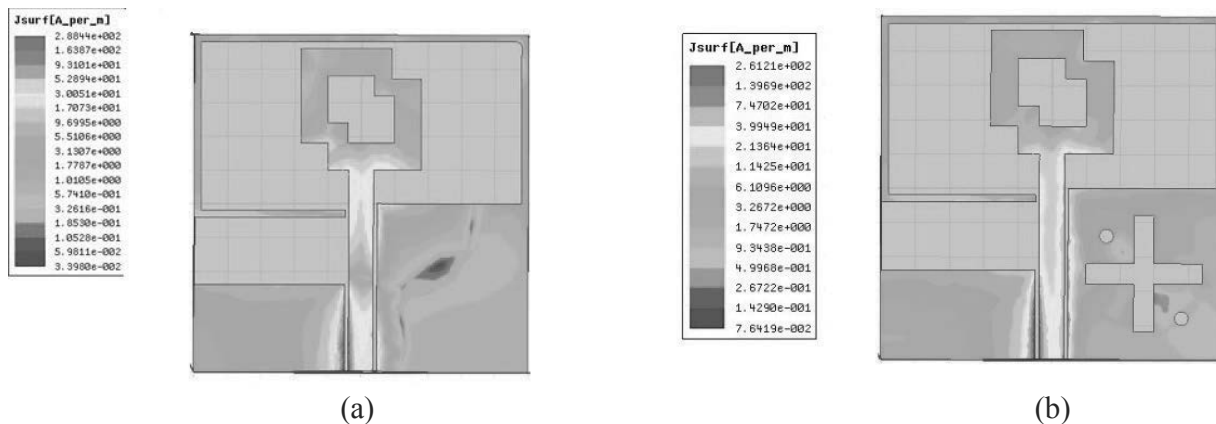


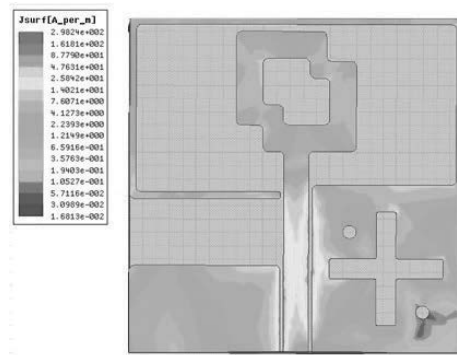
Figure 5: The 3D polar gain plot of the a) initial design b) second design c) final design

As it is mentioned before and shown in figure 6(a), by comparing the results of the three steps, in the first design (uncomplicated one) most of current is concentrated throughout the signal strip due the creation of capacitive load at a point and other parts of the antenna share a small portion of it.

At the second step by adding the plus-shape and the circle cuts to the ground plane, the surface wave distribution becomes more homogeneous on that area, figure 6(b).

As it is shown in the figure 6(c), in the last step, by rounding all the edges of the antenna a much better surface current distribution comparing to the first design is achieved.





(c)

Figure 6: Surface current distribution of the a) initial design b) second design c) proposed antenna

Figure 7 Compares the Axial Ratios of all three antennas designs. As the figure indicates, Circular polarization frequency range of the first antenna is very small, for the second antenna with plus-shaped and circular slots in the ground plane it is from 3.08GHz to 3.90GHz. While Circular polarization frequency range of the final antenna is from 3.10GHz to 4.9GHz.

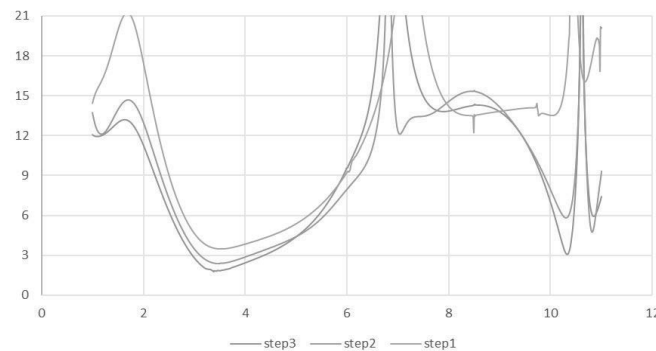


Figure 7: The comparison between Axial Ratios of the three antenna designs

Finally, A comparison has been made between the proposed antenna and some other antenna designs from the reference part in terms of dimensions, gain and operation frequency band. The related results are shown in table 1. As it is obvious from the table, the proposed antenna has a way better characteristics than most of them.

Table 1: Comparison of some References designs with proposed antenna in term of dimensions, gain and operation frequency band

Reference	Dimension	Operating Frequency	Gain
[8]	30x30x1.6	2.69-2.71GHz	3dB
[9]	70x70x1.6	1.84-2.08GHz	3.5 dB
[10]	100x100x1.6	3-4.5GHz	3.5dB
[11]	60x60x0.74	2-3GHz	3-4dB
Proposed Antenna	50x50x0.8	1.5-7GHz	5dB

4. CONCLUSION

In this work, CPW micro-strip line feed C-band antenna is designed. The simulation and design of this antenna was done in the High Frequency Structural Simulator (HFSS) software. This antenna is very small with the overall size of 50×50 mm. This antenna is designed on FR4 substrate with the thickness of 0.8mm. The operation frequency range is from 1.6GHz to 7GHz which could cover the C-band frequency range. In conclusion this survey was initially started with an uncomplicated design of micro-strip patch antenna. Later, some other changes in the initial design have been made in order to minimize the effects of unwanted frequency bands and improve the general performance of the antenna. And at the final stage, an optimized design of CP micro-strip patch antenna was achieved which is suitable for C-band (4GHz-8GHz) applications such as satellite communications, some Wi-Fi devices, wireless telephones, surveillance and weather radar systems.

REFERENCES

- [1] Constantine A. Balanis, Antenna Theory: Analysis and Design, 3rd Edition, Copyright 2005 by John Wiley & Sons, Inc. All rights reserved. Published by John Wiley & Sons, Inc., Hoboken, New Jersey. Published simultaneously in Canada, 2005
- [2] Kumar, Girish, Ray, KP, Broadband Microstrip Antennas, Artech House, UK, 2008
- [3] Karamzadeh, S., and M. Kartal. "Circularly polarised MIMO tapered slot antenna array for C-band application." Electronics Letters 51, no. 18 (2015): 1394-1396.
- [4] Karamzadeh, Saeid, and Mesut Kartal. "Circularly polarized 1× 4 square slot array antenna by utilizing compacted modified butler matrix and branch line coupler."

- International Journal of RF and Microwave Computer-Aided Engineering 26.2 (2016): 146-153.
- [5] Karamzadeh, S., et al. "Circularly polarised array antenna with cascade feed network for broadband application in C-band." *Electronics Letters* 50.17 (2014): 1184-1186.
 - [6] Design of CPW-Fed Circularly-Polarized Antenna with Cross Tuning Stub for WLAN/ISM Band Applications Sandeep Kr Singh, Rajendra Singh, Himanshu Parashar, Vepakomma Kavya Department of ECE, SET, Sharda University, Greater, Published: March.2018
 - [7] B. T. P. Madhav, H. Khan, S. K.Kotamraju, "Circularly polarized slotted aperture antenna with coplanar waveguide fed for broadband applications,"*Journal of Engineering Science and Technology* Vol. 11, No. 2,pp. 267 -277, 2016
 - [8] Lin, Y. F., H. M. Chen, and S. C. Lin, "A new coupling mechanism for circularly polarized annular-ring patch antenna," *IEEE Trans. Antennas Propag.*, Vol. 56, 11-16, Jan. 2008.
 - [9] Chou, C. C., K. H. Lin, and H. L. Su, "Broadband circularly polarized cross-patch-loaded square slot antenna," *Electron Lett.*, Vol. 43, 485-486, 2007.
 - [10] Tseng, L. Y. and T. Y. Han, "Microstrip-fed circular slot antenna for circular polarization," *Microwave Opt. Technol. Lett.*, Vol. 50, 1056-1058, Apr. 2008.
 - [11] Sze, J. Y. and C. C. Chang, "Circularly polarized square slot antenna with a pair of Inverted-L grounded strips," *IEEE Trans Antennas and Wireless Propagation Lett.*, Vol. 7, 149-151, 2008.



IJEMME

Received: 11.05.2019

Accepted: 15.06.2019

Synthetic Aperture Radar Signal Processing

Abubakar YAOUBA¹, Necip Gökhan KASAPOĞLU²

Abstract - Synthetic aperture radar signal processing is a two-dimensional operation consisting of the range compression and the azimuth compression. SAR signal processing is very important for generating and processing of various data products for different applications and analysis of the target features. The SAR raw data are 2D array of sampled echoes in complex form. The practicality of the algorithms for SAR signal processing are used to compress the energy of the echoes, thereby increasing the resolution of the SAR image. In this work, it is shown how the Range-Doppler and Stolt Interpolation techniques are carried out. The implementation of the differential azimuth compression (DAC) for the Stolt Interpolation algorithm is presented and analyzed. The Range-Doppler and Stolt Interpolation algorithms are demonstrated in Matlab and compared.

Keywords: Range-Doppler algorithm, Stolt Interpolation algorithm, differential azimuth compression, Range Cell Migration Correction, matched filter, Pulse Compression technique

1.0 Introduction

Synthetic Aperture Radar (SAR) is a type of remote sensing technology where the radar uses the motion of a small real radar antenna mounted on a moving platform such as airplanes, satellites, high altitude balloons, UAVs or drones to synthetically produce a high-resolution 2D or 3D images of objects such as landscapes. It generates and transmits a series of coded pulses at a regular interval as the platform moves along its path. The total distance the SAR device covers at a time when the radar pulses return to the antenna creates a large synthetic antenna aperture. That is, a large virtual antenna is synthesized using the displacement of the real antenna along the track. SAR operates in the microwave band, and it interacts with the target and then collects the corresponding echoes followed by imaging. SAR remote sensing is an active remote sensing technique that provides a fine spatial resolution 2D data. Fine resolution is independent of the altitude of the sensor, so images with the same geometric resolution can be obtained from the satellite as from airplanes. SAR's day-and-night imaging capability, weather independence, penetration of radar wave, geometric resolution and independence of distance, makes it one of the most popular imaging system for remote sensing.

¹ <https://orcid.org/0000-0002-8437-8064>

² Department of Electrical and Electronics Engineering, Istanbul Aydin University, Istanbul, Turkey, gokhankasapoglu@aydin.edu.tr, <https://orcid.org/0000-0001-9649-4751>

2.0 Radar modulation techniques

Radars are able to determine the distance of an object from their sensors. They are also capable to determine the speed of a moving object. This can be done by timing the delay from when the chirp signal is transmitted and to when the echo signal is received, or by determining the frequency difference between the transmitted chirp signal and the echo signal. The timing of the pulse delay employs the AM technique while the detection of the frequency difference and ranging employ the linear FM technique.

2.1 Frequency modulation (FM) technique.

In Frequency modulation (FM) technique the frequency of the carrier is varied in accordance with some characteristic of the baseband modulating signal $S_b(t)$

$$S(t) = A_0 \exp \left[j(\omega_c t + \alpha \int_{-\infty}^t S_b(t) dt) \right]$$

Since baseband-modulating signal $S_b(t)$, is normally a sinusoidal function, then

$$S(t) = A_0 \exp \left[j(\omega_c t + \alpha \int_{-\infty}^t \cos(2\pi f_a t) dt) \right] = A_0 \exp[j(2\pi f_c t + \alpha \sin \omega_a t)] \quad (1)$$

Where α is the maximum value of the phase deviation and is known as modulation index. f_c is the carrier frequency. By differentiating the instantaneous phase of $S(t)$, we obtain the instantaneous frequency f , as

$$f = 1/2\pi \frac{d}{dt} \left[\omega_c t + \alpha \int_{-\infty}^t S_b(t) dt \right] = f_c + \frac{1}{2\pi} \alpha S_b(t) \quad (2)$$

2.2 Linear Frequency Modulation (LFM) technique.

The transmitter frequency is either continually increasing or continually decreasing from the reference frequency. The transmitted FM is modified in order to be linear with time.

From the instantaneous frequency obtained in equation 2.

$$f = f_c + \frac{1}{2\pi} \alpha S_b(t) = f_c + k_r t,$$

Where $\alpha S_b(t) = 2\pi k_r t$ and k_r is known as the chirp rate (frequency changing rate) and is given as,

$$k_r = df/dt$$

Therefore $S(t) = A_0 \exp \left[j(\omega_c t + \alpha \int_{-\infty}^t S_b(t) dt) \right] = A_0 \exp \left[j(\omega_c t + \int_{-\infty}^t 2\pi k_r t dt) \right]$

$$S(t) = A_0 \exp(j2\pi f_c t + j\pi k_r t^2) \quad (3)$$

There are two common forms of LFM used in radar application: the chirp or the Pulsed LFM and the continuous-wave LFM.

2.3 The Pulsed Linear Frequency Modulation (PLFM) Radar

Lets $p_1(t)$ be defined as

$$p_1(t) = \text{Rec}\left(\frac{t - \tau_p/2}{\tau_p}\right)$$

Where the rectangular $\text{rect}(t)$ is defined as

$$\text{rect}(t) = \begin{cases} 1, & |t| \leq \frac{1}{2} \\ 0, & |t| > \frac{1}{2} \end{cases}$$

and let $p_2(t) = A_0 \exp[j(2\pi f_c t + \pi k_r t^2)]$

The Pulsed symmetrical LFM signal $S(t)$ with pulse duration τ_p is gotten as follows;

$$\begin{aligned} S(t) &= p_1(t) \cdot p_2(t - \tau_p/2) \\ &= \text{Rec}\left(\frac{t - \tau_p/2}{\tau_p}\right) \cdot A_0 \exp\left(j2\pi f_c (t - \tau_p/2) + j\pi k_r (t - \tau_p/2)^2\right) \end{aligned} \quad (4)$$

and the Pulsed nonsymmetrical LFM signal $S(t)$ with pulse duration τ_p as;

$$S(t) = p_1(t) \cdot p_2(t) = \text{Rec}\left(\frac{t - \tau_p/2}{\tau_p}\right) \cdot A_0 \exp(j2\pi f_c t + j\pi k_r t^2) \quad (5)$$

The figures below show the time–frequency relation of a pulsed LFM

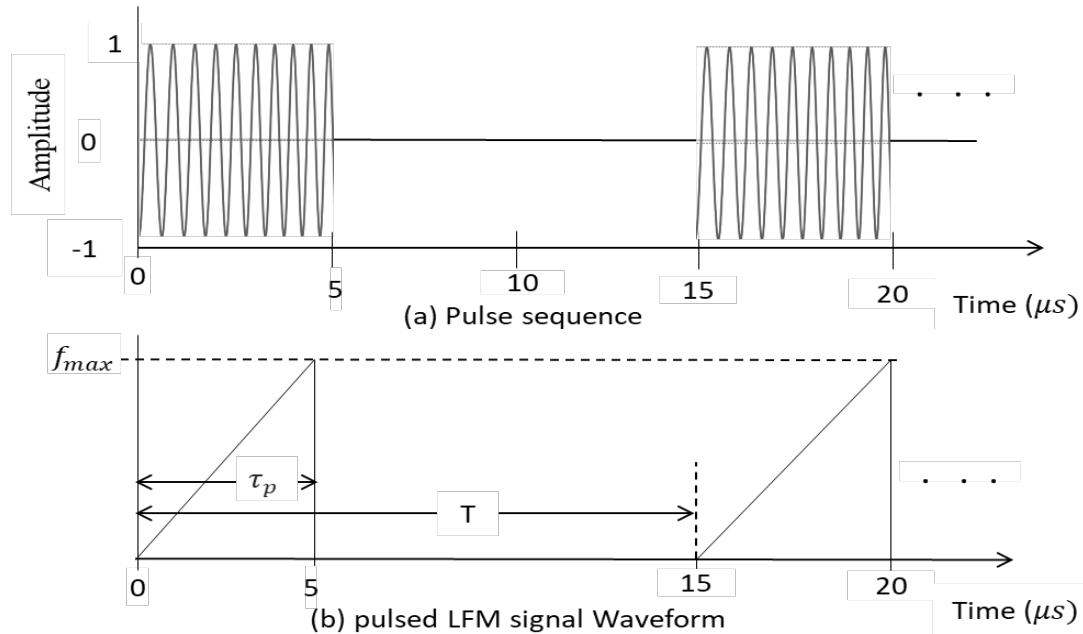


Figure 1. Lear FM pulsed train

The pulsed LFM waveform has pulse duration time τ_p where $f_{max} = k_r \tau_p$ and the frequency bandwidth is

$$B = f_{max} = k_r \tau_p \quad (6)$$

2.4 Quadrature Demodulator

Considering the LFM signal $S(t) = A_0 \exp(j2\pi f_c t + j\pi k t^2)$

The real value of the signal is represented as

$$S(t) = A_0 \cos(2\pi f_c t + \pi k t^2) = A_0 \cos(2\pi f_c t + \phi(t)) \quad (8)$$

Where $\phi(t) = \pi k t^2$ is the phase term presented for illustration purposes. The carrier frequency f_c generally has a higher value as compared to kt . The time varying-phase $\phi(t)$ information is transmitted using the complex-valued signal. After transmitting the time-varying phase $\phi(t)$ information, the Quadrature demodulator is then used to acquire the correct phase information. As illustrated on figure 2 the in-phase–quadrature-phase demodulator splits any complex-valued LFM signal $s(t)$, into the real or in-phase (I), and imaginary or quadrature-phase Q, components of $\phi(t)$. Two carriers $\cos(2\pi f_c t)$ and $\sin(2\pi f_c t)$ are locally generated by the system. The LPF filter out high frequency component $4\pi f_c t + \phi(t)$ and retain the low-frequency component $\phi(t)$. The A/D converter digitizes the real and imaginary parts of the low frequency phase signal $\phi(t)$ to obtain a complex number pair that serves as a row element of the two dimensional image the radar data.

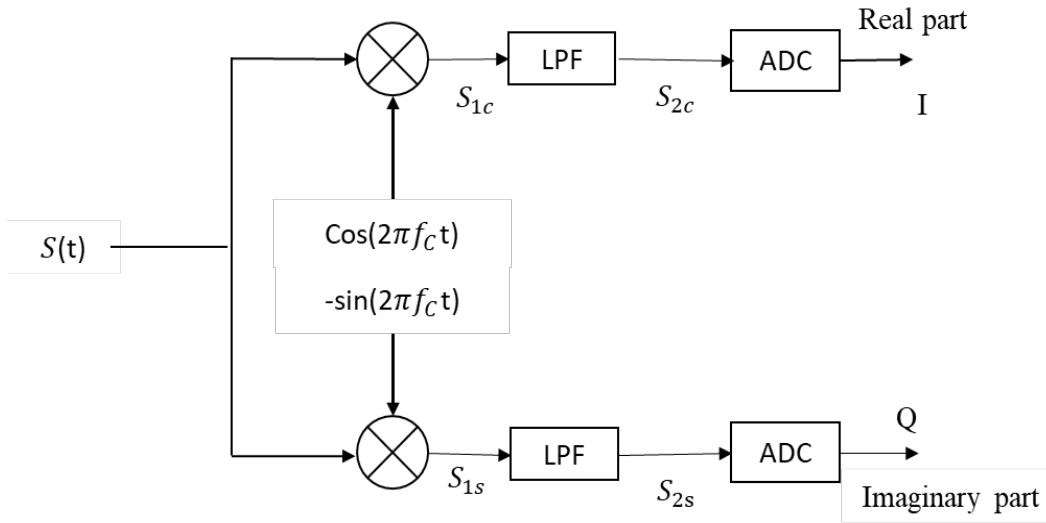


Figure 2 Quadrature demodulator

The following intermediate signals S_{1s} , S_{1c} , S_{2s} and S_{2c} are obtained as follows:

$$S_{1c}(t) = \frac{1}{2} (\cos(4\pi f_c t + \phi(t)) + \cos(\phi(t))),$$

$$S_{1s}(t) = \frac{1}{2} (\sin(4\pi f_c t + \phi(t)) + \sin\phi(t)),$$

$$S_{2c}(t) = \frac{1}{2} \cos(\phi(t)),$$

$$S_{2s}(t) = \frac{1}{2} \sin(\phi(t)).$$

The time varying signal phase $\phi(t)$ can then be obtained as:

$$\phi(t) = \tan^{-1} \left(\frac{S_{2s}(t)}{S_{2c}(t)} \right) \quad (9)$$

2.5 Matched Filter and Pulse Compression technique

Matched filtering is a technique used to regain a signal that was corrupted by additive white Gaussian noise. A matched filter is applied on received signal in order to identify a target by determining whether the filter output (compressed pulse), exceeds a specific threshold. Different targets produce pulses of different magnitudes and each magnitude depends on three factors: targets reflectivity (σ), pulse width (τ_p) and range (R) from the radar sensor to target. The effective width of a compressed pulse is determined by the bandwidth and the pulse width τ_p of the received signal

Considering an ideal target with reflectivity 1 and zero signal attenuation between the radar sensor and target area. If the input signal is $x(t)$ and the Fourier transform of the input signal is $X(f)$, then the matched filter $h(t)$ and the Fourier transform of the matched filter $H(f)$ can be expressed as follows:

$$h(t) = x^*(t) \quad \text{and} \quad H(f) = X^*(f)$$

If $f(t)$ is the output of the matched filter, then

$$F(f) = X(f)H(f) = |X(f)|^2$$

Therefore $f(t) = \mathcal{F}^{-1}(|X(f)|^2) = x(t) * h(t) = \int x(\tau)h(t - \tau)d\tau$

For $h(t) = x^*(t)$, then, $f(t) = \int x(\tau)x^*(t + \tau)d\tau$.

This is the definition of autocorrelation of $x(t)$. That is the matched filtering of any signal $x(t)$ is equivalent to the autocorrelation of that signal $x(t)$ with itself. Consider the echo of a non-symmetric LFM signal $S(t)$ to be the echo signal from single target:

$$S(t) = \text{Rec}\left(\frac{t - \tau_p/2}{\tau_p}\right) \cdot A_0 \exp(j2\pi f_c t + j\pi k t^2)$$

If $A_0 = 1$ and $h(t) = x^*(t)$, then the output of the matched filter is given as:

$$f(t) = \int_0^{\tau_p} s(\tau)s^*(t + \tau)d\tau = [-j(2\pi f_c t + \pi k t \tau_p + \pi k t^2)] \cdot T \cdot \text{sinc}(k t \tau_p) \quad (10)$$

Since convolving of two signals in the time domain is same as multiplying the two signals in the frequency domain, therefore, the matched filter will be implemented by first transforming the received signal and the matched filter function into frequency domain using Fast Fourier Transform. The resulting product of the frequency domain functions are then converted back to time domain by applying Inverse Fast Fourier Transform. Matched filter function is shorter than the received signal because of different ranges of different targets. For this reason, paddings with zeros on the matched filter function is required when applying the Fast Fourier Transform on the matched filtering. Figure 3 below shows the block diagram of DFT-based pulse compression process.

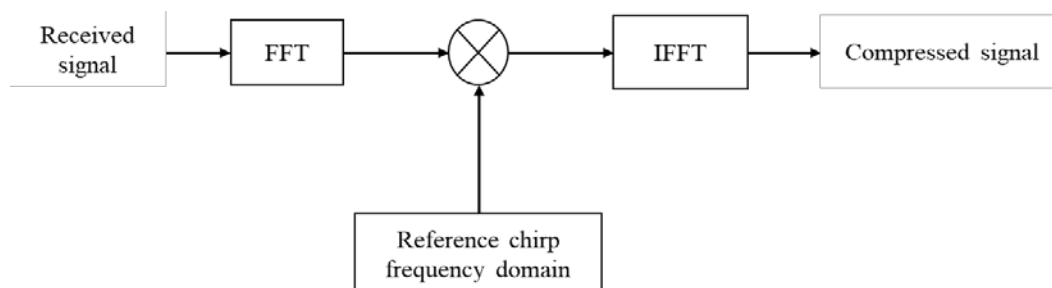


Figure 3 Block diagram of DFT-based pulse compression

3.0 SAR raw data generation

From equation 5, the PLFM radar waveform:

$$S(t) = \text{Rec}\left(\frac{t-\tau_p/2}{\tau_p}\right) \cdot A_0 \exp(j2\pi f_c t + j\pi k_r t^2)$$

With a rectangular gate function $\left(\frac{t}{\tau_p}\right)$, pulse duration time τ_p , amplitude of transmitted signal A_0 , and PLFM chirp rate k_r . The chirp signal starts and end at $t = 0$ and τ_p respectively. Let suppose the gate function is $\alpha(t)$ and the amplitude A_0 as 1. Considering the echoes are from I different reflectors, with reflective coefficient σ_i corresponding to ranges R_i , where $i = 1, 2, 3, \dots, I$, then the signal $S(t)$ written as the sum of delayed echoes is

$$\begin{aligned} S(t) &= \sum_{i=1}^I \sigma_i \alpha\left(t - \frac{2R_i}{c}\right) \cdot \exp\left\{j2\pi f_c \left(t - \frac{2R_i}{c}\right) + j\pi k_r \left(t - \frac{2R_i}{c}\right)^2\right\} \\ &= \sum_{i=1}^I \sigma_i \alpha(\mathbf{t} - \boldsymbol{\tau}_i) \cdot \exp\{j2\pi f_c (\mathbf{t} - \boldsymbol{\tau}_i) + j\pi k_r (\mathbf{t} - \boldsymbol{\tau}_i)^2\} \end{aligned} \quad (11)$$

Where $\tau_i = \frac{2R_i}{c}$ is the echo delay time from the i th target. Considering that the target location at any point (x_i, y_i) with radar the position at $(0, 0)$ at an altitude 0, then τ_i can be calculated as:

$$\tau_i = 2 \left(\frac{R_i}{c}\right) = 2 \left(\frac{\sqrt{x_i^2 + y_i^2}}{c}\right) \quad \text{and the range is calculated as } R_i = \frac{1}{2}(c\tau_i)$$

The baseband signal $S_b(t)$ can be obtained through the quadrature demodulation process by first removing the frequency of the carrier and applying a low pass filter (LPF). The demodulated baseband signal can be obtained as:

$$S_b(t) = \sum_{i=1}^I \sigma_i |\alpha(t - \tau_i)|^2 \exp\{-j2\pi f_c \tau_i + j\pi k_r (t - \tau_i)^2\}$$

If η is the time index of the demodulated signal, then the baseband signal $S_b(t)$ can be express in terms of n as:

$$S_b(\mathbf{t}_\eta) = \sum_{i=1}^I \sigma_i |\alpha(\mathbf{t}_\eta - \boldsymbol{\tau}_i)|^2 \exp\{-j2\pi f_c \tau_i + j\pi k_r (\mathbf{t}_\eta - \boldsymbol{\tau}_i)^2\} \quad (12)$$

with $\eta = 0, 1, 2, \dots, N-1$. Where N is the total number of range samples receive. N is a function pulse duration time, number of targets, and sampling frequency. The signal in 12. is based on a single pulse duration transmitted from a single position. Suppose the radar is moving along the azimuth direction (direction perpendicular to the radar beam) emitting signal at pulse repetition frequency f_{PRF} , then a two dimensional received data array will be obtain.

Suppose the moving radar position along the azimuth is u_m , where $m = 1, 2, 3, \dots, M$. with M as the total number of processed azimuth lines and must be greater than or equal to the number of azimuth lines (N_{az}) within the length L_s (synthetic aperture).

Therefore, 12. written in 2D is:

$$S_b(\mathbf{u}_m, \mathbf{t}_\eta) = \sum_{i=0}^I \sigma_i |\alpha(\mathbf{t}_\eta - \boldsymbol{\tau}_{u_m i})|^2 \exp\{-j2\pi f_c \tau_{u_m i} + j\pi k_r (\mathbf{t}_\eta - \boldsymbol{\tau}_{u_m i})^2\} \quad (13)$$

Where $\tau_{u_m i} = 2 \left(\frac{R_{u_m i}}{c}\right)$ is the received signal delay time from the i th target with radar located at the position u_m

4.0 SAR Synthesis Algorithms

The received 2D data array synthesized from the waveform of 13 has a waveform of size M by N in both azimuth and the range (time) directions. The 2D data array is formed by M bursts of the radar pulse with N samples each. The data spread in range is caused by the time duration of the transmitted PLFM signal while the spread in azimuth is due to the fact that the target is under illumination by the radar beam during which the radar is collecting echoes in a period which the radar covers the synthetic aperture length L_s .

The main aim of processing raw data is to convert it into a single pixel in the final processing stage. There exist a number of SAR signal processing techniques. Each and every SAR signal processing technique has its advantages and disadvantages. Some of these SAR signal processing techniques which are based on matched filters include; Range-Doppler, Wave domain, Omega-K, Chirp Scaling, Spectral Analysis, Stolt interpolation. The Range-Doppler technique, the Stolt-interpolation technique and the Chirp scaling technique are implemented and discussed in this work. Each of these techniques has its own advantages in high-quality imaging or computation efficiency. For instance, the Range-Doppler technique is an accurate approximation and computationally efficient for processing radar images while Stolt interpolation technique is computationally intensive, but has advantages over the Range-Doppler technique.

4.1 Range-Doppler processing of SAR data.

There are three major tasks when processing SAR data by implemented the typical Range-Doppler processor: firstly, the range compression, followed by the cell migration correction, and lastly the azimuth compression. The range Doppler technique is displayed in figure 4

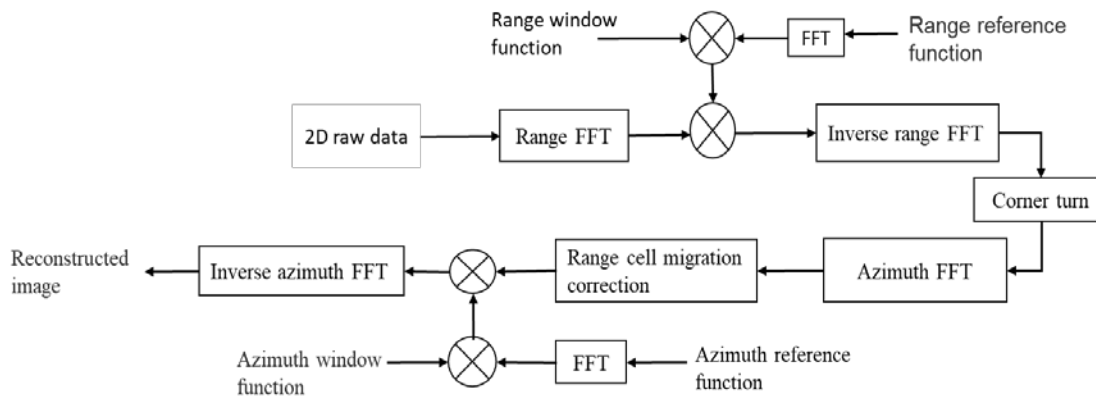


Figure 4. A flow diagram of the Range-Doppler algorithm.

The 2D raw data (complex data) refers to the quadrature demodulated baseband signal. The range compression is done in three steps. First by applying the range Fourier transform on the 2D complex data using the range FFT block, followed by Fourier transforming the range reference function using the FFT block and multiplying with each row of the Fourier transformed 2D complex data and lastly the is inversely Fourier Transformed using the range IFFT block. The 'corner turn' transpose the range 2D range compressed complex data from row data to column data for subsequent azimuth compression. The transposed 2D complex data is Fourier transformed to Range-Doppler domain using the azimuth FFT block. If range cell migration correction is required, then it is applied at this stage. To compress the data in azimuth, first the azimuth reference function is Fourier transformed using the FFT block and multiplied with each row of the 2D complex data in range Doppler domain and lastly followed by taking inverse azimuth FFT of the product. After azimuth compression, the resulting image is the constructed image of targets that were focused.

4.2 Stolt interpolation processing of SAR data

Figure 5. display the block diagram of Stolt interpolation processing of SAR raw data.

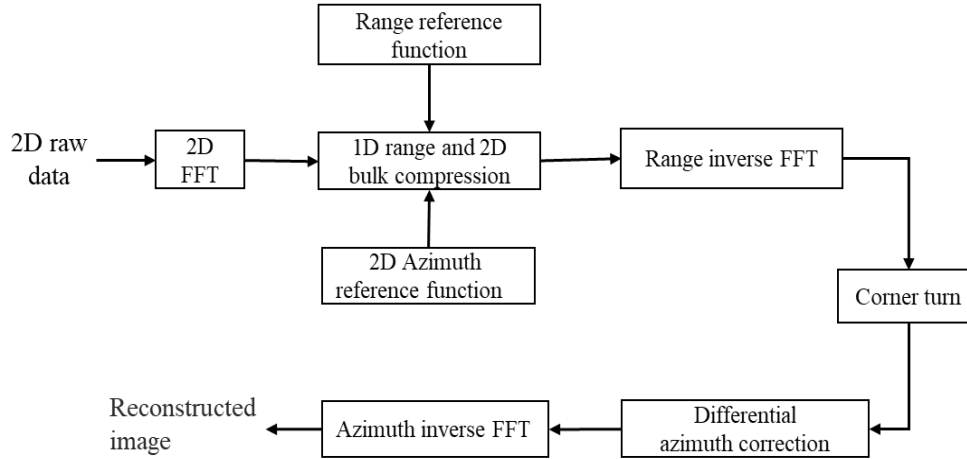


Figure 5 The diagram of Stolt interpolation algorithm processing.

4.3 Reconstruction algorithm for Stolt interpolation processing.

To compress the data in range, the 2D raw data $S_{\sigma}(t, u)$ is 2D Fourier transformed to $S_{\sigma}(\omega, \omega_{dp})$. The 2D Fourier Transformed signal $S_{\sigma}(\omega, \omega_{dp})$, will then be multiplied with the range matched filter $P_{\sigma}^*(\omega)$ to obtain a range compressed data $S_{\sigma c1}(\omega, \omega_{dp})$. The range compressed data array $S_{\sigma c1}(\omega, \omega_{dp})$ is then transformed in range–Doppler frequency domain data $S_{\sigma c1}(t, \omega_{dp})$ by taking inverse-Fourier-transformed of $S_{\sigma c1}(\omega, \omega_{dp})$.

For azimuth compression, the corresponding azimuth matched filter is obtained in following two ways:

1. By applying 1D azimuth matched filter in slow time t . With frequency changing rate k_a and the Doppler frequency f_{dp} ($f_{dp}=0$, for broadside case), the reference function is obtained as follows:

$$h_{af}(t) = \exp(-j\pi k_a t^2),$$

where the frequency changing rate $k_a = -2V^2/\lambda R_0$ and $\Delta t = 1/f_{PRF}$

The reference function $H_{af}(\omega_{dp})$ is obtained by taking FFT on $h_{af}(t)$.

2. By applying the 2D azimuth matched filter. The 2D azimuth matched filter is obtained as follows:

$$H_{af}(\omega, \omega_{dp}) = \exp \left[j \sqrt{4 \left(\frac{\omega^2}{c^2} \right) - \left(\frac{\omega_{dp}^2}{V^2} \right)} X_C \right]$$

Where ω_{dp} is the Doppler frequency in azimuth direction and ω is the time domain signal passband frequency, that is $\omega_c - \omega_0 \leq \omega \leq \omega_c + \omega_0$, where ω_c and $2\omega_0$ are the carrier frequency, and the bandwidth of the transmitting signal respectively. The distance X_C , of the radar from the center of the swath is invariant in the coordinates of the radar $(0, u)$ in stripmap SAR.

In broadside SAR, the 2D azimuth matched filter $H_{af}(\omega, \omega_{dp})$ is approximated to 1D azimuth match filter $H_{af}(\omega_{dp})$ since no range migration correction is needed while in squint SAR both the 1D and 2D reference functions are applied since it require range migration correction. Azimuth compression is carried out by multiplying each column of the range compressed data $S_{\sigma c1}(t, \omega_{dp})$ with the azimuth matched $H_{af}(\omega_{dp})$ to obtain 2D compressed data $S_{\sigma c}(t, \omega_{dp})$. After the

azimuth compression, the resulting 2D compressed signal $S_{\sigma c}(t, \omega_{dp})$ is a roughly compressed signal along azimuth direction, since only one azimuth reference function is required to perform azimuth compression on the whole data. The 2D azimuth compressed data $S_{\sigma c}(t, \omega_{dp})$ will next be processed by Stolt interpolation. Stolt interpolation improves the quality the image through differential azimuth compression based on.

$$S'_{\sigma c}(x, k_y) = S_{\sigma c}(x, k_y) \exp \left[-j \left(\frac{k_y^2}{4k_c} \right) \Delta x_n \right]$$

The differential azimuth compression requires the computation of the following terms;

First the computation of range difference $\Delta x_n = (x_n - X_c)$ where X_c and x_n are the range values along the range axis. The range difference Δx_n can be calculated as

$$\Delta x_n = c/f_s (n - N_r),$$

where N_r corresponds to the range sample at X_c

Second the computation of the constant phase $k_y^2/4k_c$, where $k_c = \omega_c/c$ and the azimuth value $k_y = 2\pi m f_{PRF}/VN_y$, with $m = 1, 2, 3, \dots, N_y$.

For a given m value along the Doppler-frequency axis, the value of k_y is computed first then followed by the multiplication of every range sample $S_{\sigma c}(t, \omega_{dp})$ by $\exp \left\{ -j \left(\frac{k_y^2}{4k_c} \right) \Delta x_n \right\}$.

After the differential azimuth compression is applied, the final image data is obtained by taking the azimuth inverse FFT with respect to ω_{dp} .

5.0 Reconstruction of satellite radar Image using Range-Doppler processing and Stolt Interpolation algorithm.

A satellite-based (ERS) raw data generated by ESA, processed and distributed by German Aerospace Center, DLR will be used in reconstructing the radar image using Range Doppler algorithm. The parameters ERS SAR sensor parameters are listed on table 1.

	Parameters		Value	Unit
Parameters for range compression	Range sampling frequency	f_s	18.962468×10^6	s^{-1}
	Chirp rate	k_r	$4.18989015 \times 10^{11}$	s^{-2}
	Chirp length	τ_p	37.12×10^{-6}	s
Parameters for azimuth compression	Velocity parameter	V	7098.0194	m/s
	Wavelength	λ	0.05656	m
	Range to target at broadside time $t = 0$	R_0	852358.15	m
	Aperture time	t_a	0.6	s
	Pulse repetition frequency	PRF	1679.902	s^{-1}

Table 1. ERS sensor parameters

Figure 6 shows the ERS data. The Range Doppler technique will be applied to process the raw data.

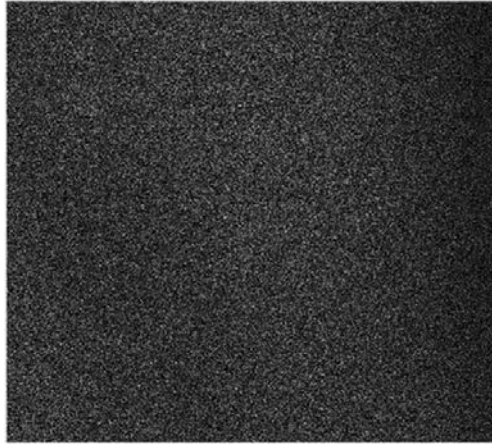


Figure 6. ERS data

The operation of range compression is performed by first transforming each row of the data into the frequency domain by applying range FFT. Since there is 704-time sample for each azimuth line, zero paddings are required for the range compression. The Fourier transformed match filter is then multiplied with every row of the frequency domain data. The range compressed data in frequency domain result is transformed back to time domain using range inverse FFT. Figure 7 shows the range compressed data.

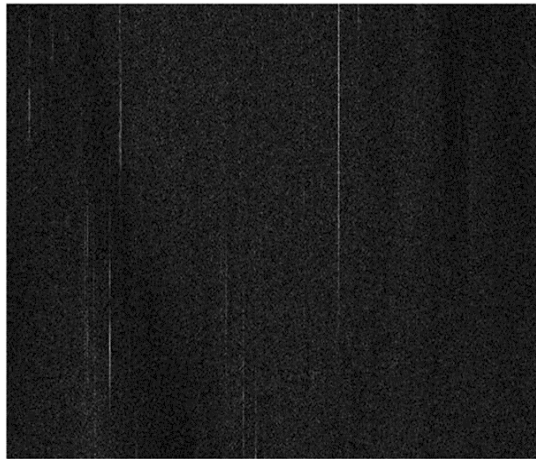


Figure 7. Range-compressed signal

To perform the azimuth compression an azimuth reference function is applied on every column of Doppler frequency domain data. First the reference function $h_{af}(s)$ is transformed into Doppler frequency domain $H_{af}(f)$ by DFT. Since the total sample number of the azimuth reference function is 1008, zero paddings are required to increase the azimuth samples number to the total length of 2048 (length of the data). The azimuth reference function $H_{af}(f)$ is next applied on every column of the data in range-Doppler frequency domain. An inverse DFT is applied on every column of the compressed data to get the processed image. The processed image is shown on Figure 8.

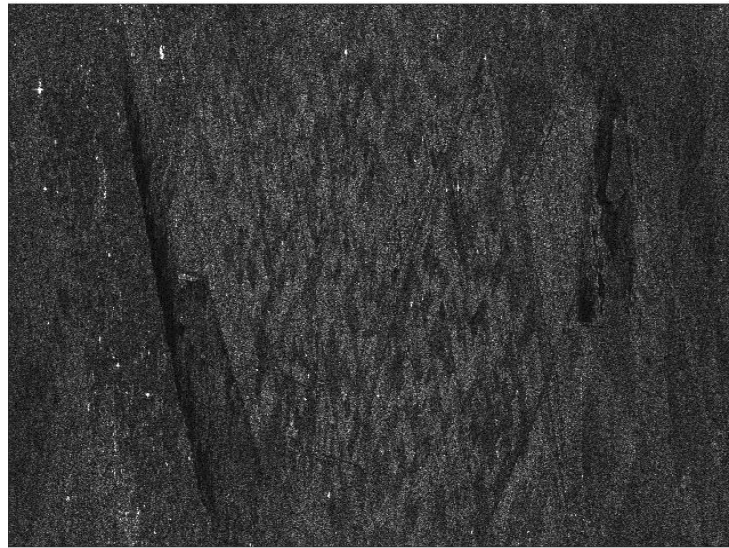


Figure 8. Constructed Image

After range compression, the next operation to perform is the azimuth compression. In azimuth compression, each column of the range compressed data and the azimuth matched filter are transformed in to Doppler frequency domain by azimuth FFT. Since The reference function $H_{af}(f)$ in Doppler frequency domain has the total number of 1008 samples, zero paddings are required to increase the azimuth samples number to the total length of 2048 (length of the data). The azimuth reference function $H_{af}(f)$ is multiplied with each column of the range-Doppler frequency domain data and the product is inversely Fourier transformed using azimuth inverse FFT to get the processed image. The processed image is shown on Figure 9.

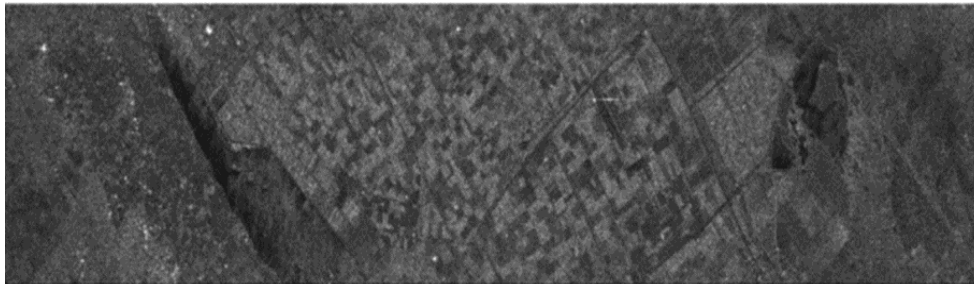


Figure 9. Image after multilook and spatial processing

To process the ERS data using Stolt interpolation, the range-compressed data array $S_{\sigma c1}(m, n')$ in figure 7 above is transformed into rang-Doppler frequency domain (t, ω_{dp}) , by applying Fourier transform on each and every column of the range compressed data array $S_{\sigma c1}(m, n')$. The compressed data in the range-Doppler frequency domain (t, ω_{dp}) , will then be processed by Stolt interpolation based on wavenumber domain.

Stolt interpolation starts by performing bulk azimuth compression using 1D and 2D azimuth matched filter and then applying differential azimuth compression. Since the ERS data provided is from broadside SAR, the 2D azimuth reference function is approximated to 1D reference function $H_{af}(\omega_{dp})$.

The range compressed data in range-Doppler frequency domain (t, ω_{dp}) is transformed to (ω, ω_{dp}) domain by applying FFT on each and every row of $S_{\sigma c1}(m, n)$ to get $S_{\sigma c1}(m', n)$ where $m' = 1, 2, 3, \dots, 2048$. The 1D azimuth reference

function is then applied to $S_{\sigma c1}(m', n)$ to obtain a roughly compressed signal $S_{\sigma c2}(m, n)$ in (ω, ω_{dp}) domain. Applying a 2D inverse FFT on the bulk compressed data $S_{\sigma c2}(m, n)$, a roughly constructed image $I_{\sigma}(m, n)$ with respect to ω , and ω_{dp} is obtained. Figure 10 displays the roughly constructed image $I_{\sigma}(m, n)$ of Stolt interpolation technique.

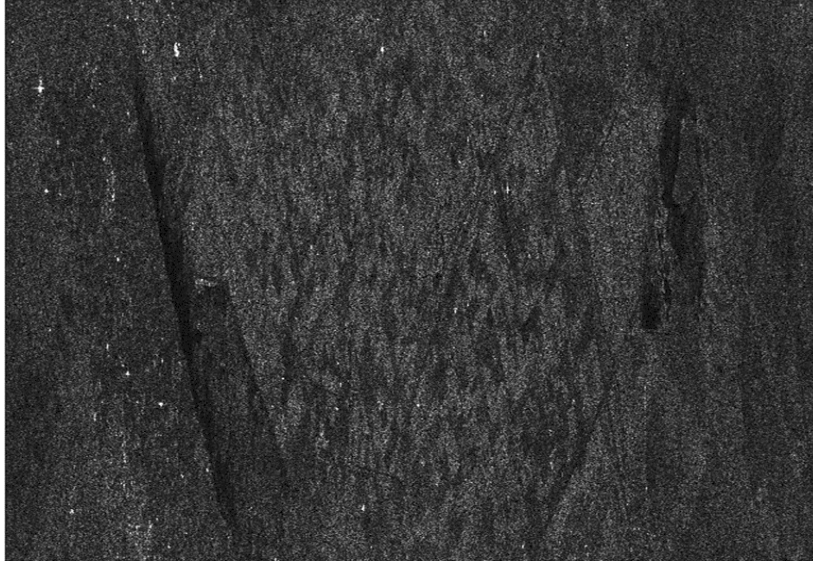


Figure 10. Processed image by Stolt interpolation technique without DAC

Comparing 10. by Stolt interpolation technique without DAC and 8 by RDA, it can be seen that the two algorithms generate images which are difficult to differentiate in terms of have quality (having similar quality). The quality of the roughly compressed image of figure 10 can further be improved by applying differential azimuth correction (DAC).

The bulk compressed data array $S_{\sigma c2}(m, n)$ in (ω, ω_{dp}) domain is inversely Fourier transformed to range Doppler frequency domain (t, ω_{dp}) before applying differential azimuth correction . To design the differential azimuth correction function, the range difference Δx_n and the phase constant k_{mc} are computed as:

$$\Delta x_n = c \left(\frac{n - N_r}{f_s} \right) \quad \text{and} \quad k_{mc} = \frac{1}{4} \left(\frac{k_y^2}{k_c} \right)$$

Where $k_y = 2\pi m f_{PRF} / V N_y$, $k_c = 2\pi f_c / c$, $m = 1, 2, 3, \dots, N_y$, $N_y = 2048$, $n = 1, 2, 3, \dots, N_x$, and the reference sample N_r , equals to the range value corresponding to the slant range R_0 (or the range sample value at X_c).

The differential azimuth function is applied on the compressed data $S_{\sigma c2}(m, n)$ for the whole range samples from 1 to 2048 as in the equation form:

$$I_{\sigma a}(m, n) = S_{\sigma c2}(m, n) \exp(-i * k_{mc} * \Delta x_n.)$$

After differential azimuth compression is computed on the roughly constructed image $I_{\sigma}(m, n)$, then inverse Fourier Transform is applied on $I_{\sigma a}(m, n)$ to obtain the final constructed image as shown in figure 11.

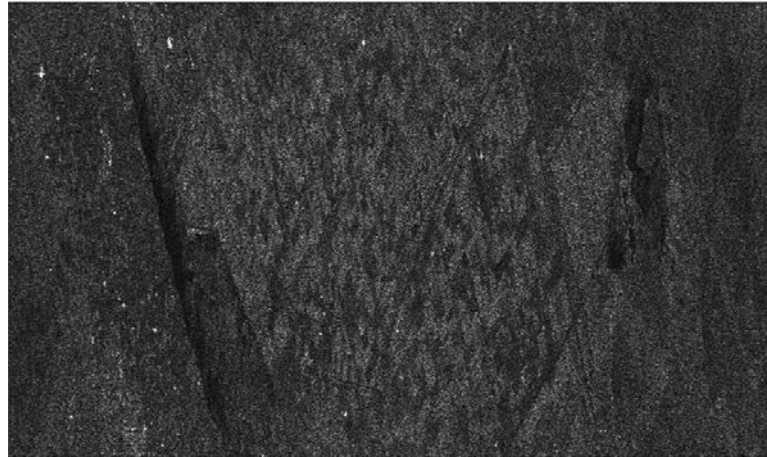


Figure 11. Processed SAR image

Applying multi-look and special filtering on the Stolt interpolation processed data, the resulting image is shown in figure 11

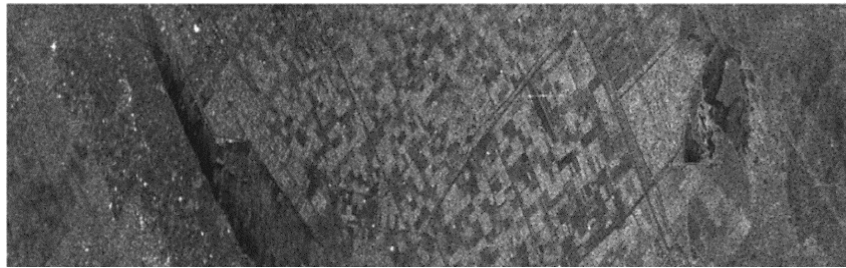


Figure 12. Image after multi-look and spatial processing

Comparing the two multi-look and spatial processed images of figure 9 and figure 12 the multi-look and spatial processing image figure 12 improves slightly in quality. This slight difference is due to the differential azimuth compression involved in the Stolt Interpolation algorithm

6.0 COMPARISON OF ALGORITHMS

The Range-Doppler algorithm is computationally efficient, flexible, less computational time and is an accurate approximation for processing of radar images but has some disadvantages with respect the high computational time to obtain good accuracy in the range cell migration correction operation. That is, it becomes computationally heavy when an accuracy in range cell migration correction is required

The Stolt interpolation algorithm is very accurate but computationally intensive due to heavy interpolation involved. It has advantages over the Range-Doppler algorithm.

7.0 CONCLUSION

This work focuses on the Range-Doppler technique and Stolt Interpolation technique in detail and their respective flow diagrams and important parameter expressions has been described in detailed. Also, the Range-Doppler technique and Stolt Interpolation technique were successfully implemented on Matlab to construct the SAR image and the two algorithms were compared.

8.0 REFERENCES

- [1] Teng Long, Cheng Hu, Zegang Ding, Xichao Dong, Weiming Tian, Tao Zeng. "Geosynchronous SAR: System and Signal Processing", Springer Science and Business Media LLC, 2018
- [2] Advances in Decision Sciences, Image Processing, Security and Computer Vision", Springer Science and Business Media LLC, 2020
- [3] Didier Massonnet, Jean-Claude Souyris Imaging with synthetic aperture radar
- [4] Frdric Adragna. "Synthetic Aperture Radar Images", Processing of Synthetic Aperture Radar Images, 01/01/2008
- [5] Chen, Kunshan Principles of synthetic aperture radar signal processing
- [6] Soumekh M. Synthetic Aperture Radar Signal Processing with Matlab algorithms
- [7] Teng Long et al. Geosynchronous SAR System and Signal Processing Springer (2018)
- [8] https://saredu.dlr.de/unit/SAR_imaging
- [9] Bu-Chin Wang-Digital Signal Processing Technique
- [10] Schlutz M.-Synthetic Aperture Radar Imaging Simulated in matlab
- [11] John C. Curlander, Robert N. McDonough-Synthetic Radar Signal processing.
- [12] Walter G. Carrara, Ron S. Goodman Ronald M Majewski-Spotlight Synthetic Aperture Radar Signal Processing Algorithms.
- [13] Robert Wang, Yunkai Deng.-"Bistatic SAR System and Signal Processing Technology", Springer Science and Business Media LLC, 2018
- [14] srmmap.edu.in
- [15] Spotlight Synthetic Aperture Radar", Principles of Modern Radar Advanced techniques, 2012.
- [16] www.transint.boun.edu.tr
- [17] Wu, Huaming.-"Motion Compensation for Near-Range Synthetic Aperture Radar Applications", KIT Scientific Publishing, Karlsruhe, 2012.
- [18] Remote Sensing and Digital Image Processing, 2001
- [19] Clay Stewart.-Synthetic Aperture Radar Algorithm
- [20] Thuy Le Toan- Introduction to SAR Remote Sensing
- [21] Mark A. Richards-Fundamentals of Radar Signal Processing

INTERNATIONAL JOURNAL OF ELECTRONICS, MECHANICAL AND MECHATRONICS ENGINEERING

Submission Instructions

The scope of International Journal of Electronics, Mechanical and Mechatronics Engineering (IJEMME) covers the novel scientific papers about Electronics, Image Processing, Information Theory, Electrical Systems, Power Electronics, Control Theory, Embedded Systems, Robotics, Motion Control, Stochastic Modeling, System Design, Multidisciplinary Engineering, Computer Engineering, Optical Engineering, Design Optimization, Material Science, Metamaterials, Heat and Mass Transfer, Kinematics, Dynamics, Thermo-Dynamics, Energy and Applications, Renewable Energy, Environmental Impacts, Structural Analysis, Fluid Dynamics and related topics of the above subjects.

IJEMME is an international journal published four times a year (January, April, July and October). Manuscripts reporting on original theoretical and/or experimental work and tutorial expositions of permanent reference value are welcome. IJEMME Editorial Board is authorized to accept/reject the manuscripts based on the evaluation of international experts. The papers should be written in English.

The manuscript should be sent in electronic submission via IJEMME paper submission system of web address (www.aydin.edu.tr/ijemme)

Submission instructions of manuscripts.

Page Design: Text body area is (195mm x 275mm). 30 mm margin from top, 20 mm from down and 25 mm margin should be left on right/left sides.

Title should be in 16 pt. bold, capital letters with Times New Roman font in Microsoft Word format. Authors' names, affiliations, e-mail addresses should follow the title after double line spacing with authors' names and surnames in lower case except first letters in 14 pt, the rest is 10 pt. italic.

Abstract should not exceed 200 words with the word "Abstract" in 10 pt. italic, bold, abstract text in 9 pt. italic, all in Times New Roman font in Microsoft Word format.

Key Words not exceeding 5 should be in bold.

Document Character: Subtitles should be in 10 pt. bold, capital letters and text body 10 pt. both with Times New Roman font in Microsoft Word format. The manuscripts should be written on a single column, be double spaced with single line spacing between paragraphs. The subtitle of the first section should start after a single space following the keywords, the other subtitles also with a single line space following the text, there should also be single line spacing between the previous text and the subtitle.

Conclusion: section should have a title written in 10 pt. bold, capital letters and the text in 10 pt. all in Times New Roman font in Microsoft Word format.

Reference numbers should be given in brackets as illustrated below:

Referencing books:

[1] Özsu M., T, Valduriez, P., *Principles of Distributed Database Systems*, Prentice Hall, New Jersey, 128-136,1991.

Referencing papers:

[2] G. Altay, O. N., Ucan, “Heuristic Construction of High-Rate Linear Block Codes,” *International Journal of Electronics and Communications (AEU)*, vol. 60, pp.663-666, 2006.

Page number is to be placed at the top left corner of each page with pencil.

Length of the Manuscript should not exceed 20 pages excluding Figures and Tables.

INSTRUCTIONS ABOUT THE ACCEPTED MANUSCRIPTS:

Page Design: Text body area is (195mm x 275mm). 30 mm margin from top, 20 mm from down and 25 mm margins should be left on right/left sides.

Title should be in 16 pt. bold, capital letters with Times New Roman font in Microsoft Word format. Authors’ names, affiliations, e-mail addresses should follow the title after double line spacing with authors’ names in lower case and surnames in capital letter in 14 pt. the rest in 10 pt. in the same format.

Abstract should not exceed 200 words with the word “Abstract” in 12 pt. italic, bold, abstract text in 9 pt. italic, all in Times New Roman font in Microsoft Word format.

Key Words not exceeding 5 should be in 9 pt. bold.

Document Character: Subtitles should be in 10 pt. bold, capital letters and text body 10 pt. both with Times New Roman font in Microsoft Word format. The manuscripts should be written on two columns, be single spaced with single line spacing between paragraphs. The subtitle of the first section should start after a single space following the keywords, the other subtitles also with a single line space following the text, there should also be single line spacing between the previous text and the subtitle.

Sections: Formulas should be numbered sequentially. Referring to formulas should be as Eqn (.). Figures and Tables should be placed into the text body and captions for both should be 10 pt. Table numbers and captions should be placed before the Table. If necessary, both columns may be used for large Figures and Tables.

Conclusion section should have a title written in 12 pt. bold, capital letters and the text in 10 pt. all in Times New Roman font in Microsoft Word format. Conclusion should not be a version of the Abstract.

Reference numbers should be given in brackets as illustrated below:

Referencing books:

[1] Özsu M., T, Valduriez, P., *Principles of Distributed Database Systems*, Prentice Hall, New Jersey, 128-136,1991.

Referencing papers:

[2] G. Altay, O. N., Ucan, "Heuristic Construction of High-Rate Linear Block Codes," *International Journal of Electronics and Communications (AEU)*, vol. 60, pp.663-666, 2006.

Short Biography of the authors should follow references after a single line space, names in 9 pt. surnames in 9 pt. and the text in 9 pt. The text should not exceed 100 words.

CORRESPONDENCE ADDRESS:

Editor in Chief

Prof. Dr. Hasan Alpay HEPERKAN
Istanbul Aydın University, Faculty of Engineering
Mechanical Engineering Department
Florya Yerleskesi, Inonu Caddesi, No.38, Kucukcekmece, Istanbul, Turkey
Fax: +90 212 425 57 59 - Tel: +90 212 425 61 51 / 22001
E-mail: hasanheperkan@aydin.edu.tr

Prepared by

Instructor:Saeid KARAMZADEH
Engineering Faculty
Electrical and Electronics Eng. Dept.
Inonu Caddesi, No.38, Florya, Istanbul, TURKEY
E-mail: saeidkaramzadeh@aydin.edu.tr

Published by

Istanbul Aydın University
Graphic Design Department



KÜTÜPHANE VE BİLGİ MERKEZİMİZ 7/24 HİZMET VERİYOR



56.000
Basılı Kaynak



1.000.000
E-Kaynak



Engelsiz
Kütüphane



Mobil
Uygulamalar

24/7

- Kütüphane 7/24/365 gün hep açık
- 75.000 aylık kullanıcı
- Mimarlık ve Mühendislik Fakültesi için çizim salonları
- Galeri Aydın
- Kafeterya



instagram: kutuphaneiau



twitter.com/iaukutuphane



facebook.com/iaukutuphane